Applied Physics B (2024) 130:39
https://doi.org/10.1007/s00340-024-08172-6

Applied Physics B
Lasers and Optics

RESEARCH

Nickel–cobalt layered double hydroxide as a saturable absorber for continuous wave mode-locked laser

Long Du[1] · Chun Qi[1] · Xiaohui Hu[1] · Jianxin Zhao[1] · Guocheng Sun[1] · Fei Lou[1] · Shuaiyi Zhang[1] · Xia Wang[1,3] · Zhihong Wu[2]

Received: 27 November 2023 / Accepted: 2 January 2024 / Published online: 20 February 2024

Abstract
The nickel–cobalt (NiCo) layered double hydroxide (LDH) is prepared by ultrasonic liquid phase-assisted exfoliation method and dispersed onto mirror forming saturable absorber (SA). With NiCo-LDH SA, a continuous wave mode-locked laser at 1065.9 nm with a maximum output power of 1.72 W was achieved with a repetition frequency of 69 MHz and a pulse width of 18 ps. To the best of our knowledge, this is the first implementation of the NiCo-LDH as a SA for continuous wave mode-locked laser operation, which demonstrates the great potential of the NiCo-LDH for integration into lasers.

1 Introduction

Due to their unique characteristics including high peak power, good beam quality and low thermal impact, 1 μm ultrafast lasers have been widely applied in various fields such as optical imaging, biomedical sciences, materials processing, environmental monitoring, etc. [1–4]. Passive mode-locking based on saturable absorber (SA) modulation plays a crucial role in generating 1 μm ultrashort pulses. Compared with active mode-locking which requires external modulator, passive mode-locking has numerous advantages including simple structure, stable pulse operation, high repetition rate and fast response time [5–7].

In passively mode-locked laser, semiconductor SA mirrors (SESAMs) are commonly used due to their stability and tunability [8]. However, the SESAMs usually suffer from complex preparation process, high cost and limited application wavebands. Owing to their facile fabrication, rapid response times and adjustable bandgaps, the two-dimensional materials as SAs have been extensively studied such as graphene [9], black phosphorus (BP) [10], topological insulators (TIs) [11], transition metal dichalcogenides (TMDs) [12], etc. Graphene, a zero-bandgap material, offers a large modulation bandwidth but has a lower damage threshold. BP exhibits a wide range of tunability but is susceptible to oxidation, resulting in a poor stability in ambient air. TIs possess unique electronic band structures and surface states with high saturable absorption efficiency, but the manufacturing process remains relatively complex. TMDs have high carrier mobility and long exciton recovery time, while the intrinsic energy bandgap is between 1 and 2 eV which limits their applications in the mid-infrared wavebands.

Recently, Layered Double Hydroxides (LDHs) have attracted much attention due to their stable layered structure, large specific surface area, remarkable capacity for ion exchange and commendable tunability [13]. The efficacy of Ni-based LDHs as potential SAs in ultrafast lasers has been experimentally demonstrated. In 2021, we used a Nickel-vanadium layered double hydroxide (NiV-LDH) as SA to achieve passively Q-switched mode-locking in a 2 μm laser, generating pulses as narrow as 320 ps [14]. Subsequently, we demonstrated a 1.3 m passively Q-switched mode-locking laser based on the nickel–cobalt layered double hydroxide (NiCo-LDH) SA with a pulse width as narrow as 25 ps [15]. In 2023, Wang et al. utilized NiCo-LDH as a SA to achieve

✉ Xia Wang
phwangxia@163.com

✉ Zhihong Wu
wuzhihong@qiluhospital.com

[1] Shandong Engineering Research Center of New Optoelectronic Information Technology and Devices, School of Mathematics and Physics, Qingdao University of Science and Technology, Qingdao 266061, People's Republic of China

[2] Qilu Hospital of Shandong University, Jinan 201800, People's Republic of China

[3] School of Physics and Technology, Jinan University, Jinan 250001, People's Republic of China

a passively Q-switched mode-locking laser at 2 μm with a pulse width of 221 ps [16].

In this paper, we achieve a 1065.9 nm continuous wave mode-locked (CWML) laser with the Nickel–cobalt layered double hydroxide SA. The ultrafast laser has a repetition frequency of 69 MHz, a shortest pulse width of 18 ps and a spectral linewidth of 0.46 nm. To the best of our knowledge, this is the first demonstration of nickel-based LDH as a SA for 1-μm CWML laser operation.

2 Preparation and characterization of NiCo-LDH SA

NiCo-LDH SA is prepared with ultrasonic liquid-phase exfoliation combined with drop-casting method. Firstly, adding 40 mg NiCo-LDH powder to a 10 mL centrifuge tube, followed by the addition of 9 mL anhydrous ethanol (CH_3CH_2OH). Mixing them evenly by employing intermittent ultrasound for 12 h in an ultrasonic cleaner. Subsequently, centrifuging the mixture with 6000 revolutions per minute for 15 min. Finally, taking 60 μL of the supernatant and drop-casting it onto a plane mirror (1000–1100 HR), and drying it at room temperature for 12 h.

The Raman spectra of the NiCo-LDH excited by a 633 nm laser source is shown in Fig. 1a. The sharp peak at 526 cm^{-1} is attributed to vibrations of M–O, O–M–O and M–O–M (here, the M stands for Ni and Co) bonds. The peak at 1072 cm^{-1} originates from the C–O vibration mode of interlayer methanol molecules. The peak at 1344 cm^{-1} is ascribed to the asymmetric stretching of interlayer carbonate anions [18]. Figure 1b shows the X-ray diffraction (XRD, Rigaku, Japan) of the NiCo-LDH. The diffraction peaks were observed at 12.5, 33.76, 39.56 and 59.84 degrees, corresponding to the (003), (006), (015) and (110) planes of the LDH structure, respectively [19]. Figure 1c exhibits the atomic force microscopy (AFM, MULTIMODE8, Germany) image of the NiCo-LDH nanosheets, indicating a height of approximately 15 nm (as shown in Fig. 1d).

Figure 2a and b shows the transmission electron microscopy (TEM, HT7800, Japan) and scanning electron microscopy (SEM, JSM-6700F, Japan) images of the NiCo-LDH, respectively, indicating that the NiCo-LDH powder exhibits a banded morphology characterized by alternating layered arrangements. The composition ratios of C, O, Ni, and Co elements were measured by energy dispersive spectrometer (EDS) (SU8010, HITACHI), as shown in Fig. 2c. Figure 2d shows the EDS elemental spectroscopy of the NiCo-LDH sample, characterizing the elemental composition and distribution.

Figure 3a shows the linear transmission of NiCo-LDH, which is measured by a spectrophotometer ranging from 500 to 1500 nm. The experimental setup of the opening Z-scan is shown in Fig. 4. In the experiment, a titanium-sapphire (Ti:Sapphire) laser with a repetition frequency of 80 MHz, a pulse width of 56 fs and a central wavelength of 800 nm was utilized as the light source. Two plano-convex lenses with a focal length of 200 mm were used to focus light

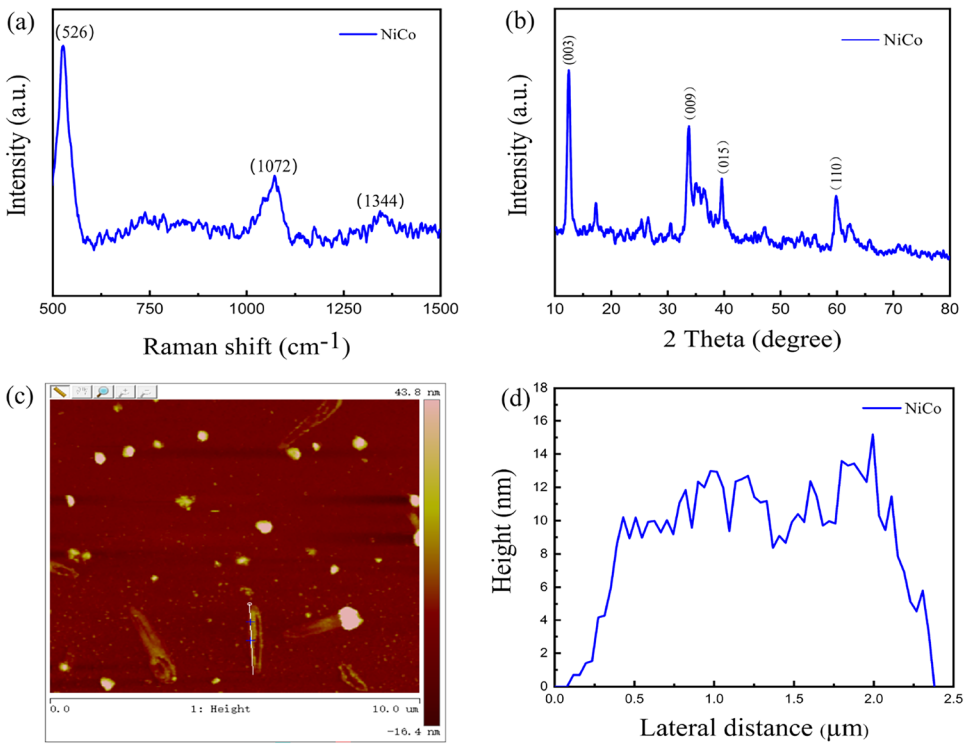

Fig. 1 **a** Raman spectra of the NiCo-LDH powders; **b** XRD pattern of the NiCo-LDH powders; **c** AFM image and **d** corresponding height distribution of the NiCo-LDH nanosheet

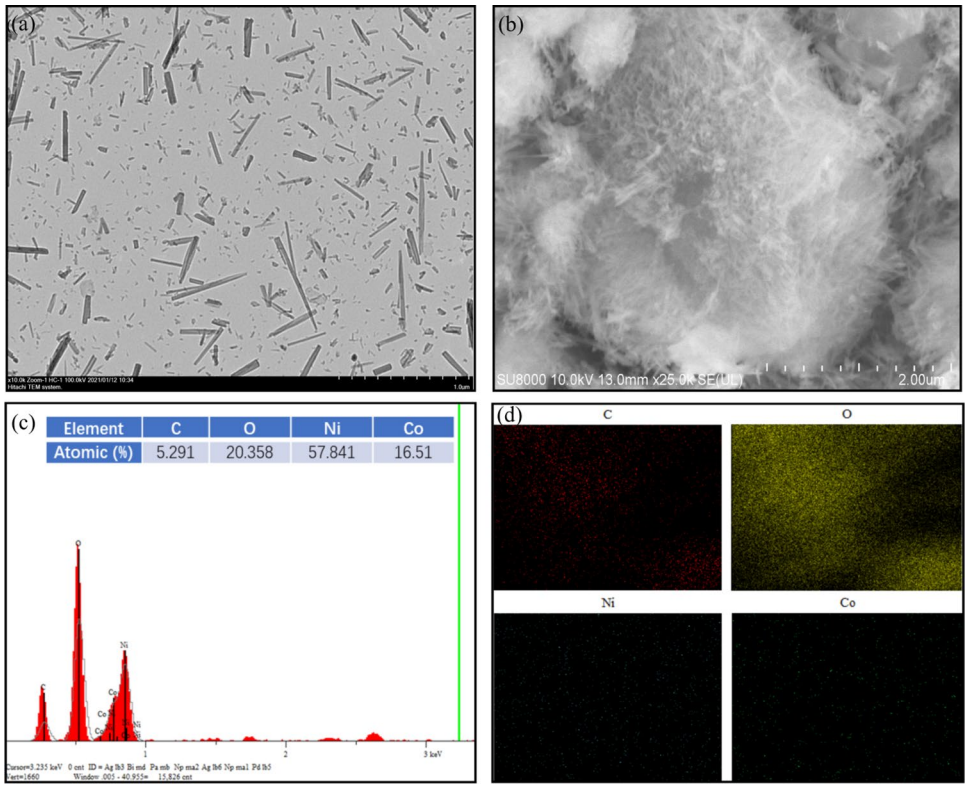

Fig. 2 **a** TEM image of the NiCo-LDH; **b** SEM image of the NiCo-LDH; **c** EDS image of the NiCo-LDH; inset: Percentage of elements in the NiCo-LDH; **d** EDS elemental mapping images of the NiCo-LDH

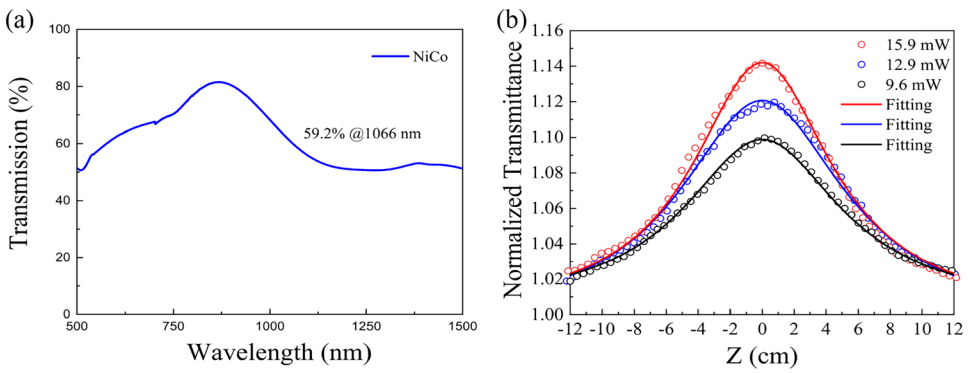

Fig. 3 **a** Wavelength-dependent changes in linear transmittance spectrum of the NiCo-LDH; **b** Open aperture Z-scan curves

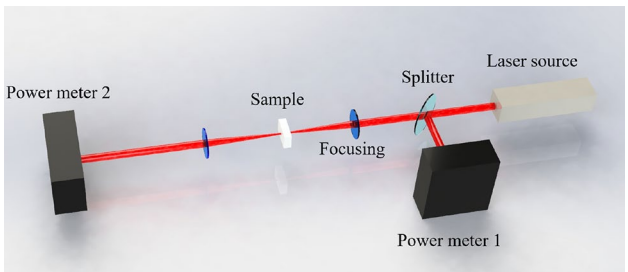

Fig. 4 Z-scan experimental setup

spots. The beam was divided into two identical beams with the beam splitter and two identical power meters was used to record the power before and after passing through the NiCo-LDH SA. The transmittances of the sample at different positions were recorded to test the nonlinear absorption characteristics of the NiCo-LDH SA, as shown in Fig. 3b. The results show that the transmittance variation with the Z-scan is symmetrically distributed around the center of the Z-scan. The Z-scan experiments do not exhibit any instances of two-photon or multi-photon absorption, which are typical manifestations of saturation absorption phenomena. The results of the Z-scan experiment can be fitted using the following formula [20],

$$T = \sum_{m=0}^{\infty} \frac{\left[-q_0(z,0)\right]^m}{(m+1)^{1.5}}, m \in N, \quad (1)$$

$$q_0(z,0) = \frac{\beta_{\text{eff}} L_{\text{eff}} I_0}{\left(1 + \frac{Z^2}{Z_0^2}\right)}, \tag{2}$$

where $T(z)$ is the transmission, $L_{\text{eff}} = (1 - e^{-\alpha_0 L})/\alpha_0$, L_{eff} is the sample's effective thickness, I_0 is the on-axis irradiance at the focus, Z_0 is the diffraction length of the beam. The open aperture Z-scan experimental results indicate the saturable absorption of NiCo-LDH. The nonlinear absorption coefficient is − 1.1 cm/GW [21].

3 Experimental setup and results

The experimental setup of the passively mode-locked Nd:YVO_4 laser is depicted in Fig. 5, which is a "W" type resonator with a cavity length of 2.1 m. The pump source is a fiber-coupled semiconductor laser with a central wavelength of 808 nm. Through a 1:1 coupling system, the pump laser is focused into the laser medium. The laser medium is a $3\times3\times6$ mm^3 Nd:YVO_4 crystal with a doping concentration of 0.5 at. %. Both end faces of the crystal are coated with an antireflection (AR) at 808 nm and 1064 nm. To dissipate heat loading, the Nd:YVO_4 crystal is wrapped with indium foil and then placed into a copper hot sink cooling with 10 °C circulating water. A flat mirror (M1) is placed in front of the crystal as the input mirror with coating with AR at 808 nm and high reflection (HR) at 1064 nm. Two concave mirrors (M2, M3) with a curvature of 500 mm serve as the folded mirror of the W-shaped cavity, which is coated with HR at 1000–1100 nm on the inner surface. The end of the W-cavity is also a flat mirror (M4) with a HR coating at 1000–1100 nm. Additionally, the NiCo-LDH SA is placed in the cavity. The output mirror is a concave mirror with a curvature of 100 mm (M5) with a transmittance of 10% at 1064 nm.

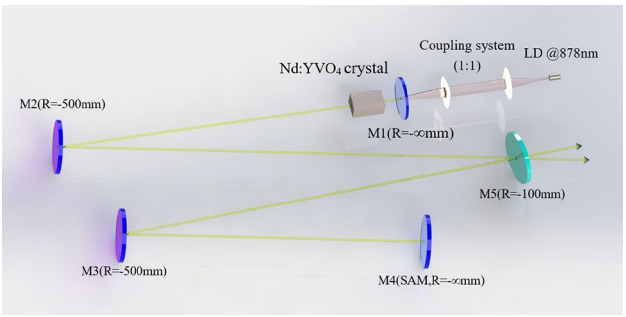

Fig. 5 The experimental setup of passively mode-locked Nd:YVO_4 laser with NiCo-SA

The average output power was measured by the power meter (Thorlabs, S302C). The output pulses were monitored by an oscilloscope (Agilent Technologies, DSO-X3104A) with a photoelectric probe (EOT, ET-3000). The laser spectrum was recorded by a spectrometer.

As shown in Fig. 6a, the laser threshold is about 0.4 W. The maximum average output power of 1.72 W was achieved with a slope efficiency of 22% under the absorbed pump power of 8.29 W. The central wavelength is located at 1065.9 nm with a narrow spectral linewidth of 0.46 nm. To evaluate the stability of CWML average output power, a power meter was used to document power variations over time, as shown in Fig. 6b. Average output power values were systematically recorded at one-second intervals over a 1-h period. Notably, with the absorbed pump power (P_{abs}) maintained at 8.29 W, the observed variation in average output power remained below 1.5%. We maintained CWML laser operation for seven hours, and the pulse profile observed on the oscilloscope remained stable. When the laser was shut down and restarted after 1 week, a subsequent oscilloscope check confirmed the good stability of the CWML laser in our experiment.

The pulse train of 1 μm mode-locked laser is depicted in Fig. 7. When the pump power located at a lower level, Q-switched mode-locking (QML) pulses appear (as shown in Fig. 7a, b) with repetition frequency of 69 MHz, corresponding to a cavity round-trip length of 4.2 m. According to the mode-locking theory, the achievement

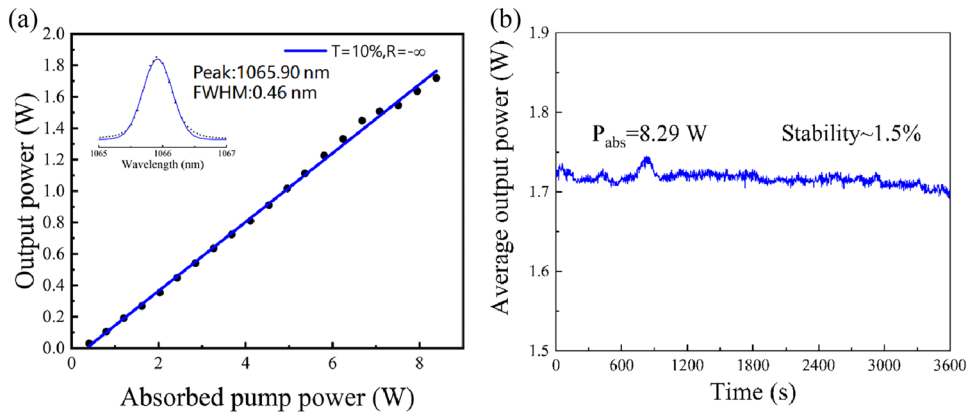

Fig. 6 **a** Average output power of the passively mode-locked Nd:YVO_4 laser. Inset: the corresponding laser spectrum; **b** Average output power fluctuations over time

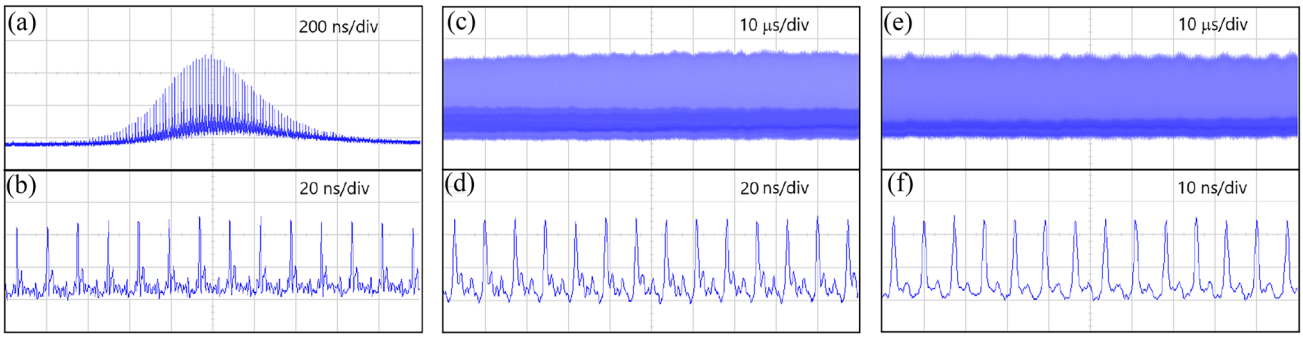

Fig. 7 **a** and **b** The temporal pulse train in the QML state; **c** and **d** The temporal pulse train in the CWML state; **e** and **f** The temporal pulse train of second harmonic wave in the CWML state

of CWML necessitates that the pulse energy within the cavity should be satisfied as Eq. (3) [22]:

$$E_{p,c} = \sqrt{F_{\mathrm{sat},L} A_{\mathrm{eff},L} F_{\mathrm{sat},A} A_{\mathrm{eff},A} \Delta R}. \quad (3)$$

$E_{p,c}$ is the minimum intra-cavity pulse energy which is required for obtaining stable CW mode locking, $F_{\mathrm{sat},L}$ is the saturation flux of the gain medium and can be calculated with $F_{\mathrm{sat},L} = h\upsilon/2\sigma_L$ (σ_L, which is equal to 11.4×10^{-19} cm^2, is the emission cross-section of the Nd:YVO_4 crystal @1064 nm), $A_{\mathrm{eff},L}$ and $A_{\mathrm{eff},A}$ is the area of the fundamental mode in the Nd:YVO_4 crystal and the NiCo-LDH SA mirror, respectively, $F_{\mathrm{sat},A}$ is the saturation energy density of the SA mirror, ΔR is the modulation depth of the NiCo-LDH SA. A stable CWML is achieved for $E_p > E_{p,c}$ and a QML is achieved for $E_p < E_{p,c}$.

As the pump power increases, the energy in the cavity is large enough to generate CWML pulses, as shown in Fig. 7c, d. The CWML pulses have a pulse repetition rate of 69 MHz, corresponding to the cavity round-trip time. Under certain conditions, an intra-cavity SA can support not only fundamental wave mode-locking (a single pulse per cavity round trip) but also harmonic wave mode-locking (several pulses per cavity round trip), as shown in Fig. 7e, f [21].

The pulse width of CWML pulses was measured by an autocorrelator (A.P.E, Pulse check 50). Figure 8 shows the autocorrelation trace of the 1 μm CWML pulses, which have a pulse width of 18 ps with a Gaussian Fitting.

Table 1 summarizes the relevant reports of solid-state mode-locked lasers using nickel-based LDH as SAs. To our knowledge, this is the first demonstration of the NiCo-LDH as a SA for CWML operation.

Table 2 summarizes the results for 1 μm solid-state CWML lasers using a variety of 2D material SAs. Notably, the output power achieved by using NiCo-LDH as SA is higher than other 2D materials. This remarkable performance provides compelling evidence for the potential utility of NiCo-LDH SA in high-power ultrafast mode-locked laser systems.

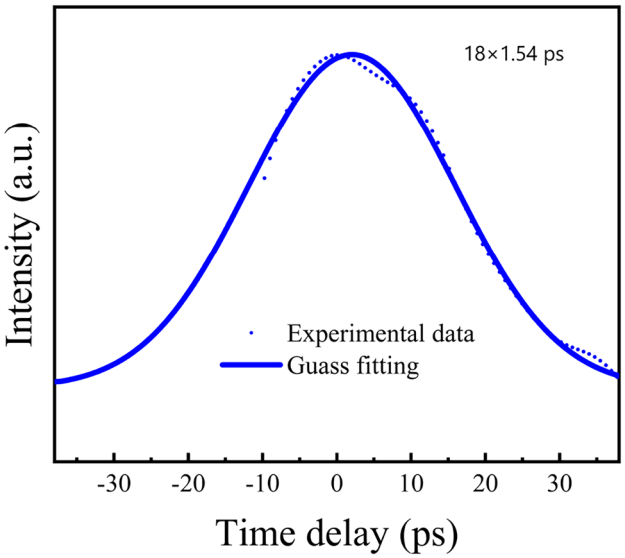

Fig. 8 Autocorrelation trace (Gaussian pulse shape assumed)

4 Conclusion

In conclusion, the NiCo-LDH SA was successfully prepared by ultrasonic liquid phase-assisted exfoliation method. Based on the NiCo-LDH SA, a W-type Nd:YVO_4 all-solid-state mode-locked laser was achieved with a maximum output power of 1.72 W, a pulse width of 18 ps and a repetition frequency of 69 MHz. The results reveal that the NiCo-LDH

Table 1 Mode-locked laser based on nickel-based LDH

SAs	Gain medium	Type	Wavelength (μm)	Pulse width (ps)	Repetition frequency (MHz)	References
NiCo-LDH	Nd:$Lu_{0.15}Y_{0.85}VO_4$	QML	1.3	25	134	[15]
NiCo-LDH	Tm:YAG ceramic	QML	2	221	146	[16]
NiV-LDH	Tm:YAG ceramic	QML	2	320	145	[14]
NiCo-LDH	Nd:YVO_4	CWML	1	18	69	This work

Table 2 Performance summary of CWML solid-state lasers operating in 1 μm with 2D material

SAs	Gain medium	Central wavelength (nm)	Pulse width (ps)	Repetition frequency (MHz)	Output power	References
Graphene	Nd:$GdVO_4$	1064	16	43	360 mW	[23]
Graphdiyne	Nd:YVO_4	1064.4	23	92.9	1.27 W	[24]
Nb_2C	Nd:YVO_4	1063.9	13.5	99.1	426 mW	[25]
2D Te	Nd:YVO_4	1064.3	5.8	100.3	852 mW	[26]
$PtSe_2$	Nd:$LuVO_4$	1066	15.8	61.3	180 mW	[27]
BP	Nd:YVO_4	1064	6.1	140	460 mW	[28]
MoS_2/GO	Nd:$GdVO_4$	1064	17.15	1.02	508 mW	[29]
NiCo-LDH	Nd:YVO_4	1065.9	18	69	1.72 W	This work

SA possesses excellent potentials for ultrashort 1 μm pulse laser generation.

Acknowledgements This work was supported by the National Natural Science Foundation of China (No. 12174211, 12174212).

Author contributions Conceptualization, CQ methodology, LD software, XH validation, FL formal analysis, CQ investigation, XH resources, FL and SZ data curation, JZ and GS writing—original draft preparation, LD writing—review and editing, LD visualization, FL supervision, SZ and ZW project administration, XW and ZW funding acquisition, SZ and XW. All authors have read and agreed to the published version of the manuscript.

Data availability Data underlying the results presented in this paper are not publicly available at this time but may be obtained from the authors upon reasonable request.

Declarations

Conflict of interest The authors declare no conflicts of interest.

References

1. Y. Abe, K. Meguriya, T. Matsuzaki et al., Micromanipulation of amyloplasts with optical tweezers in Arabidopsis stems[J]. Plant Biotechnol. **37**(4), 405–415 (2020). https://doi.org/10.5511/plantbiotechnology.20.1201a
2. R.W. Waynant, I.K. Ilev, I. Gannot, Mid–infrared laser applications in medicine and biology[J]. Philos. Trans. R. Soc. Lond. Ser. A: Math. Phys. Eng. Sci. **359**(1780), 635–644 (2001). https://doi.org/10.1098/rsta.2000.0747
3. E. Khalkhal, M. Rezaei-Tavirani, M.R. Zali et al., The evaluation of laser application in surgery: a review article[J]. J. Lasers Med. Sci. **10**(Suppl 1), S104 (2019). https://doi.org/10.15171/jlms.2019.S18
4. Z. Xue, F. Shen, J. Li et al., MEMS modulator-based mid-infrared laser heterodyne radiometer for atmospheric remote sensing[J]. Front. Phys. **10**, 945995 (2022). https://doi.org/10.3389/fphy.2022.945995
5. J. Bogusławski, Y. Wang, H. Xue et al., Graphene actively mode-locked lasers[J]. Adv. Func. Mater. **28**(28), 1801539 (2018). https://doi.org/10.1002/adfm.201801539
6. M. Li, S. Zhao, K. Yang et al., Diode-pumped actively Q-switching and mode-locking Nd:$GdVO_4$ laser[J]. Laser Phys. Lett. **5**(10), 722–725 (2008). https://doi.org/10.1002/lapl.200810065
7. F. Lou, X. Cui, X. Sheng et al., Large-diameter indium antimonide microwire based broadband and robust optical switch[J]. Sci. China Phys. Mech. Astron. **66**(2), 224211 (2023). https://doi.org/10.1007/s11433-022-1969-9
8. A. Diebold, T. Zengerle, C.G.E. Alfieri et al., Optimized SESAMs for kilowatt-level ultrafast lasers[J]. Opt. Express **24**(10), 10512–10526 (2016). https://doi.org/10.1364/OE.24.010512
9. Q. Bao, H. Zhang, Y. Wang et al., Atomic-layer graphene as a saturable absorber for ultrafast pulsed lasers[J]. Adv. Func. Mater. **19**(19), 3077–3083 (2009). https://doi.org/10.1002/adfm.200901007
10. P.C. Debnath, K. Park, Y.W. Song, Recent advances in black-phosphorus-based photonics and optoelectronics devices[J]. Small Methods **2**(4), 1700315 (2018). https://doi.org/10.1002/smtd.201700315
11. Y.Y. Lin, P. Lee, J.L. Xu et al., High-pulse-energy topological insulator Bi_2Te_3-based passive Q-switched solid-state laser[J]. IEEE Photonics J. **8**(4), 1–10 (2016). https://doi.org/10.1109/JPHOT.2016.2581490

12. Q.H. Wang, K. Kalantar-Zadeh, A. Kis et al., Electronics and optoelectronics of two-dimensional transition metal dichalcogenides[J]. Nat. Nanotechnol. **7**(11), 699–712 (2012). https://doi.org/10.1038/nnano.2012.193
13. Y. Liang, Y. Liu, W. Qiao et al., Optical nonlinearity and laser modulation performance of FeNi-LDH in the mid-infrared region[J]. Opt. Lett. **46**(10), 2348–2351 (2021). https://doi.org/10.1364/OL.426287
14. E. Cai, X. Kong, S. Zhang et al., Nickel-vanadium layered double hydroxide for a mid-infrared 2 μm Tm: YAG ceramic ultrafast laser[J]. Appl. Opt. **61**(20), 6057–6061 (2022). https://doi.org/10.1364/AO.462620
15. E. Cai, J. Xu, Y. Liu et al., Passively Q-switched and Q-switched mode-locked Nd:$Lu_{0.15}Y_{0.85}VO_4$ lasers at 1.34 μm with a nickel-cobalt layered double hydroxide saturable absorber[J]. Opt. Mater. Express **12**(3), 931–939 (2022). https://doi.org/10.1364/OME.447019
16. M. Wang, Y. Xu, Z. Yu et al., Nickel–cobalt layered double hydroxide saturable absorber for a mid-infrared 2 μm Tm:YAG ceramic mode-locked laser[J]. Appl. Phys. B **129**(7), 104 (2023). https://doi.org/10.1007/s00340-023-08051-6
17. L. Sun, L. Zhang, H.J. Yu et al., 880 nm LD pumped passive mode-locked TEM_{00} Nd: YVO_4 laser based on SESAM[J]. Laser Phys. Lett. **7**(10), 711 (2010). https://doi.org/10.1002/lapl.201010051
18. T. Wang, S. Zhang, X. Yan et al., 2-Methylimidazole-derived Ni–Co layered double hydroxide nanosheets as high rate capability and high energy density storage material in hybrid supercapacitors[J]. ACS Appl. Mater. Interfaces **9**(18), 15510–15524 (2017). https://doi.org/10.1021/acsami.7b02987
19. X. Gao, Z. Jia, B. Wang et al., Synthesis of NiCo-LDH/MXene hybrids with abundant heterojunction surfaces as a lightweight electromagnetic wave absorber[J]. Chem. Eng. J. **419**, 130019 (2021). https://doi.org/10.1016/j.cej.2021.130019
20. X. Zhang, A. Selkirk, S. Zhang et al., MoS_2/carbon nanotube core–shell nanocomposites for enhanced nonlinear optical performance[J]. Chem. Eur. J. **23**(14), 3321–3327 (2017). https://doi.org/10.1002/chem.201604395
21. E. Cai, J. Xu, Y. Xia et al., The nonlinear optical properties of Zirconium pentatelluride and its application in ultrafast solid-state lasers[J]. Opt. Laser Technol. **150**, 108003 (2022). https://doi.org/10.1016/j.optlastec.2022.108003
22. C. Hönninger, R. Paschotta, F. Morier-Genoud et al., Q-switching stability limits of continuous-wave passive mode locking[J]. JOSA B **16**(1), 46–56 (1999). https://doi.org/10.1364/JOSAB.16.000046
23. J.L. Xu, X.L. Li, Y.Z. Wu et al., Graphene saturable absorber mirror for ultra-fast-pulse solid-state laser[J]. Opt. Lett. **36**(10), 1948–1950 (2011). https://doi.org/10.1364/OL.36.001948
24. Q. Hao, J. Guo, L. Yin et al., Watt-level ultrafast bulk laser with a graphdiyne saturable absorber mirror[J]. Opt. Lett. **45**(19), 5554–5557 (2020). https://doi.org/10.1364/OL.404540
25. Z. Yang, L. Gao, H. Chen et al., Broadband few-layer niobium carbide MXene as saturable absorber for solid-state lasers[J]. Opt. Laser Technol. **142**, 107199 (2021). https://doi.org/10.1016/j.optlastec.2021.107199
26. Z. Yang, L. Han, Q. Yang et al., Two-dimensional tellurium saturable absorber for ultrafast solid-state laser[J]. Chin. Opt. Lett. **19**(3), 031401 (2021). https://doi.org/10.3788/col202119.031401
27. W. Liu, M. Liu, J. Yin et al., Tungsten diselenide for all-fiber lasers with the chemical vapor deposition method[J]. Nanoscale **10**(17), 7971–7977 (2018). https://doi.org/10.1039/c8nr00471d
28. B. Zhang, F. Lou, R. Zhao et al., Exfoliated layers of black phosphorus as saturable absorber for ultrafast solid-state laser[J]. Opt. Lett. **40**(16), 3691–3694 (2015). https://doi.org/10.1364/OL.40.003691
29. G. Zhao, J. Hou, Y. Wu et al., Preparation of 2D MoS2/graphene heterostructure through a monolayer intercalation method and its application as an optical modulator in pulsed laser generation[J]. Adv. Opt. Mater. **3**(7), 937–942 (2015). https://doi.org/10.1002/adom.201500012